CHAPTER 6

DETECTION OF STRUCTURES IN LOW RESOLUTION BIOLOGICAL ULTRASOUND IMAGES USING ACTIVE CONTOUR PRINCIPLES

JESPER BRØNDUM

SUBMITTED TO BIOIMAGING

ABSTRACT

A segmentation method specifically developed for low resolution images is presented. The method is inspired by principles from active contours and performs an iterative update of a parametric curve based on energy minimisation. The energy minimisation includes information from edge detection, curve smoothness, and correspondence with a score image from an a priori performed principal component analysis on a training set of images. Because of the score image, the segmentation is ensured to resemble the common structure of the segmentation item, but without the need of performing a parametric model of the expected shape. The method is successfully applied to the transverse images of loins from the Autofom ultrasound scanner for pork carcasses with the purpose of estimating the area. These image suffer from low resolution in one dimension (16×635 points in each image). A method for automatic detection of initial points are developed with mathematical morphology, and the active contour segmentation is proved superior to elliptic fit on the initial points in the relation to manual measured loin muscle area.

INTRODUCTION

Detection of complicated structures in industrial biological images is becoming a major subject in many applications. The industrial biological applications often differ from the medical applications in the need for immediate feed back from the image applications and the required robustness of the algorithms since no user interactions is permitted. This often compromises the precision of the segmentation. Therefore cutting edge techniques from computer vision is extensively gaining use in the biological industry often with techniques modified from the field of medical imaging. An often applied example is the tissue characterisation in medical images as in e.g. Mouroutis *et al.* (1998).

One of the approaches that has dominated the research in medical imaging in the past years is the active contours or snakes. Active contours were introduced by Kass *et al.* (1988), as a method for dynamic changes of a segmentation curve based on information from local energy and deformations, and external forces. Many papers have addressed the issue of active contours since the initial proposal. Caselles *et al.* (1997) discussed split and merge problems, Sapiro and Tannenbaum (1993) discussed simplification of the initial proposal regarding curve smoothness control and Lai and Chin (1995) discussed the problems of shape irregularity in noisy images. Blake *et al.* (1993) proposed the inclusion of both local and global model features and Gunn and Nixon (1997) extended the segmentation to two contours; one to extract and one to contract, thereby improving the robustness of the contour and making the segmentation less sensitive to initialisation. Cohen (1991) introduced the concept of 3D balloons, and worked further with finite element methods for active contour models in Cohen and Cohen (1993) and Geiger *et al.* (1995) propose the use of dynamic programming.

Thus, much effort has been put into deriving and extending theoretical concepts of active contours. However, none of the approaches has addressed the problem of low resolution in one or more of the spatial dimensions of the image. Due to a specific ultrasonic application, this issue is highly relevant. Therefore, the scope of this paper is to meet the problem of low resolution in at least one of the spatial domains with the active contour principles. To solve this problem, a general constraint based on an a-priori common structure in the images is introduced. The common structure is resolved from a principal component analysis (PCA) on a set of congruent training images. The concept of the PCA was first introduced by Pearson (1901), and was further introduced by Hotelling (1933). More recently, the technique has been used on images in e.g. Esbensen and Geladi (1989) and Geladi *et al.* (1989). In the latter the score image is used as a common structure in multivariate images obtained at different

wavelengths. In this paper, the same approach is used here to detect common structures in a set of training images appended from different objects.

The problem of current interest concerns the Autofom, a three-dimensional automatic ultrasonic scanner for carcasses in pork abattoirs as reported in Brøndum *et al.* (1998). The system captures a 16×200×635 (width×length×depth) data sequence of the entire carcass, and the resolution in the different dimensions is therefore very different. The system is mainly designed for real time grading of the carcasses based on meat percentage. The resolution in the length and depth has therefore been chosen with the highest priority. However, additional quality output from the system is requested by many users. One of the qualitative parameters that draws special attention, is the area of the loin muscle. For the abattoirs, this feature can be used to produce a more consistent product. The concept of the proposed active contour is introduced and generalised for a wider use. Finally, it is applied on the Autofom images for fully automatic segmentation of the transversal muscle structure of the loin, where the very coarse resolution (16 transverse measurements) is the essence of the problem.

METHODS

The aim of the segmentation is to detect the structure of the loin muscle in the transverse images of the Autofom ultrasound scanner. A brief introduction to the Autofom is given, and this is followed by the automatic detection of the initial points for the active contour initialisation. Finally, follows the active contour developed for the low resolution ultrasound images.

AUTOFOM ULTRASOUND IMAGES

The Autofom consists of 16 pulse-echo transducers positioned in a U-shaped frame. The carcass is automatically pulled through the frame with the transducers, with the back facing the frame. The weight of the carcass and the humidity of the skin are sufficient to ensure a reasonable contact with the transducer to produce a reasonable image quality. A measurement for every 5'th mm is made which sum up to a total of approximately 200 scans with each transducer. 2 MHz ultrasound pulses are used, and the echoes from the tissue intersections are sampled with 5 MHz. A total depth of 120 mm is measured in the media and with the estimated ultrasound velocities in fat and meat this gives a resolution of 0.15 mm. Hence the acquired three-dimensional image consists of 16×200×635 points.

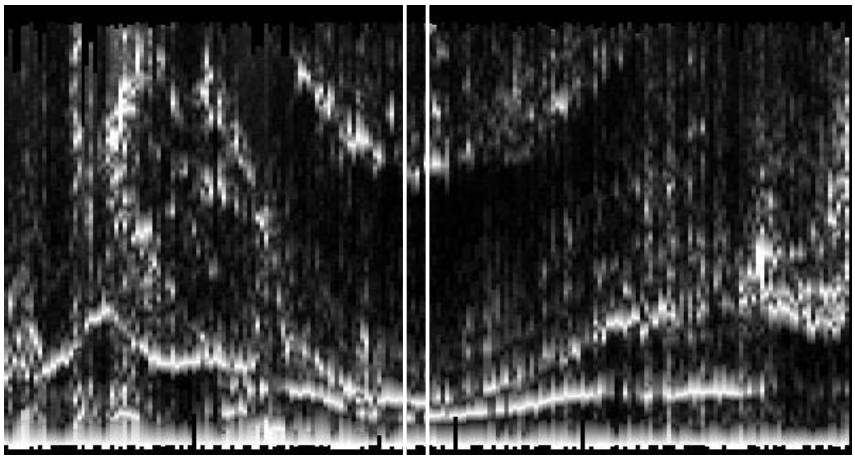

Figure 1. Longitudinal ultrasound image. The minimum skin depth (MSD) is shown at the right vertical line. The two vertical lines show mark the region where the transverse image is obtained from.

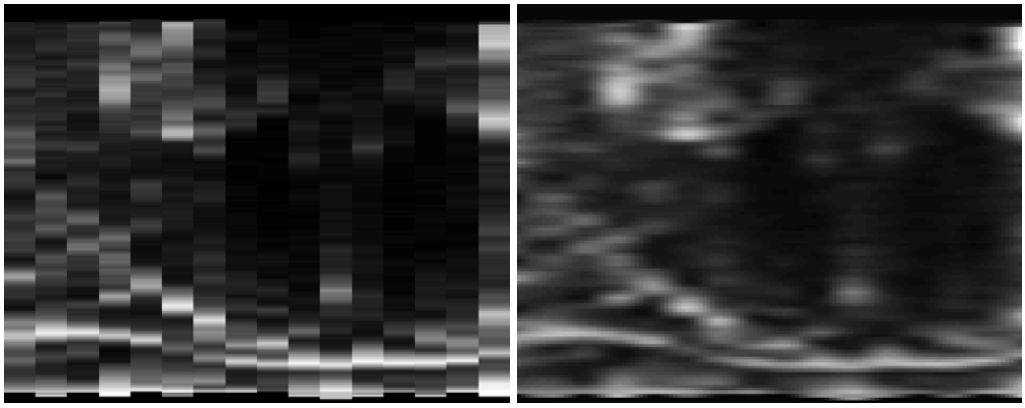

Figure 2. Transverse ultrasound images, left: with pixel replication, and right: with bipolar interpolation.

Each of the transducers generates an image in the length dimension, known as a longitudinal image (see Figure 1). The longitudinal images are used for extracting some structural features regarding the anatomy of the animals. Inspecting all 16 transducers measured at the same longitudinal position show a cross section of the carcass. The cross sectional image dimension is perpendicular to the length direction of the animal and the images in this dimension are denoted transverse images. The transverse images have a major drawbacks due to the coarse resolution in one of the directions since each of the transverse images are of size 16×635 points (see Figure 2a). The goal of the segmentation is to detect the loin muscle in the centre of the transverse image. It is important to note, that the orientation of the carcass differ for each measurement. Therefore, orientation detection is one of the primary steps in the current software of the Autofom system. Two main features are important: 1) the localisation of the minimum skin depth (MSD), and 2) the transducer where the midline (MID) of the carcass back is found. These two features are used as input to the segmentation procedure described in the following sections.

MORPHOLOGIC DETECTION OF INITIAL POINTS

Often in active contour driven applications, the initial points for the segmentation process are user supplied. Due to the concept of the Autofom being for on-line use and fully automatic, this is not applicable in the current situation. An automatic detection of the initial points is therefore developed as first part of the segmentation process.

The accuracy of morphologic operations is seldom the main reason for the use of these techniques. However, morphology is usually stable and do most often provide a solution to the segmentation problem. Therefore, morphology is used as basis for detection of the initial points in the segmentation procedure of the Autofom images.

As mentioned, the MSD and MID features are used as input to the segmentation procedure. From these characteristic points, the expected centre of the loin muscle (CLM) in the transverse image can be calculated. From the CLM, the outer border of the muscle structure is traced. This step is made by a simple grey scale morphologic operation. The search is made in a star shape oriented from the CLM, at the distance d and in the direction with the angle α with the horizontal direction in the transverse image.

Since the curvature of the loin muscle is round, a structure element, S, of varying size, depending on α, is used. At the horizontal direction of the transverse image ($\alpha=0$), S is of size 3×7 and at the vertical direction ($\alpha=\pi/2$), S is similarly of size 7×3. Generally, the size of S is given by equation 1. The intensity of S is constant and equal to 255.

$$\begin{pmatrix} S_{width} \\ S_{height} \end{pmatrix} = abs \begin{pmatrix} 3+4\sin(\alpha) \\ 3+4\cos(\alpha) \end{pmatrix} \quad (1)$$

Following the path from CLM at the angle α and using S from equation 1, the morphologic operator, $M_{d,\alpha}$, is given by equation 2, where $I_{d,\alpha}$ denoted the image at the polar coordinates (d,α) relative to CLM and $\otimes$ denotes a morphologic dilation (Gonzales and Woods 1992).

$$M_{d,\alpha} = I_{d,\alpha} \otimes S \quad (2)$$

Detection of the initial points in the direction α is done by finding the parameters d and α with the highest positive gradient of M along the path, i.e. the position with the largest increase of the morphologic operator.

ELLIPSE FITTING

A transverse cut of the loin is usually close to elliptic shape. The active contour is therefore compared to a segmentation with a least squares fit of an ellipse of the initial

points detected with the morphology. Let **x** and **y** denote two vectors with the initial points. The ellipse is then represented as given in equation 3, which is fitted with ***x*** and ***y*** in a least squares sense.

$$Ax^2 + By^2 + Cxy + Dx + Ey = 1 - F \tag{3}$$

Let φ denote the rotation of the angle of the ellipse relative to the vertical direction in the transverse image. φ can then be found as shown in equation 4.

$$\varphi = \frac{1}{2}\arctan\left(\frac{C}{A-B}\right) \tag{4}$$

The centre point of the ellipse (c_x,c_y) is found with the matrix multiplication given in equation 5.

$$(c_x, c_y) = \begin{bmatrix} D & E \end{bmatrix} \begin{bmatrix} 2A & C \\ C & 2B \end{bmatrix}^{-1} \tag{5}$$

Similarly, the radii of the ellipse, *a* and *b*, are found with equation 6.

$$(a,b) = \sqrt{\frac{\begin{bmatrix} 2 \\ 2 \end{bmatrix}}{\begin{bmatrix} 1+A+B \\ 1+A+B \end{bmatrix} \frac{C}{\sin(2\varphi)}}} \tag{6}$$

Now, the ellipse can be represented by φ, c_x, c_y, *a*, and *b*. The features output from the ellipse fitting algorithm are the area, the perimeter, *a*, and *b*.

ACTIVE CONTOUR

The principle of active contours are founded on an energy minimisation along the contour of a parametric defined curve. Kass *et al.* (1988) originally introduced the energy function along the curve, C, given in equation 7.

$$E(C) = \alpha \int_0^1 |C'(q)|^2 \, dq + \beta \int_0^1 |C''(q)|^2 \, dq - \lambda \int_0^1 |\nabla I(C(q))| dq \tag{7}$$

where α, β, and λ are real and positive constants. The two first terms are related to the internal curve energy, and the third term relates to extracting the curve towards the image object. Among others, Caselles *et al.* (1997) discussed that the curve smoothness can be obtained even with β=0, and equation 8 can therefore be reduced to equation 6.

$$E(C) = \alpha \int_0^1 |C'(q)|^2 \, dq - \lambda \int_0^1 |\nabla I(C(q))| dq \tag{8}$$

Hereby the active contour is simplified to an edge detector (from the second term) with conserved curve smoothness (from the first term). However, equation (8) lacks

the possibility of including an a priori knowledge of the shape of the object structure. This is especially relevant for the current application where the resolution in the width dimension is poor and the risk that the edge detection task fails is high. The a-priori structure is included by relating *C* to the primary score image from a principal component analysis (PCA) of a training set. The score image obtains low intensities in the areas with common intensities and high intensities in areas with high variation. The intensities of the score image are rescaled to the level -127 to 128, which is expected to minimise the error along the most common structure of the loin muscles in a set of images. Due to the different orientation in the images, it is important that the images are aligned by their CLM. Integration of the error contribution from the PCA score image along C is introduced in as the third term in Equation 9.

$$E(C) = \alpha \int_0^1 |\, C'(q)\,|^2 \; dq - \lambda \int_0^1 |\, \nabla I(C(q))\,| dq + \varepsilon \int_0^1 |\, PC(C(q))\,| dq \qquad (9)$$

where ε is a positive constant, and PC is the score image from the PCA aligned spatially by the centre of the initial points. The third term minimises the risk that the active contour will not grow to an unrealistic size and shape.

The implementation of the active contour is made by using a spline approximation of C using a set of vertices at a given resolution. The vertices of the initial curve C_0 are found from the initial points. The curve smoothness is estimated by the squared gradient of C_0 at a resolution of 0.001. The edge detection is estimated using a Canny operator (see e.g. Russ 1994) on the ultrasound image along C_0. The succeeding curves, C_i, are updated iteratively by the steepest descent method. No other stopping criteria than a maximum number of iterations has been used for this application. At a later stage, where the processing time can be critical, a dynamic criteria depending on the minimised error should be implemented.

RESULTS AND DISCUSSION

Totally 100 images have been measured manually for the LMA detection. This is done with a comprehensive visual inspection using a grid plastic sheet. The measurements have been made by a trained meat quality inspector at a commercial abattoir in the US. Only the right side of the carcass is measured, and due to the orientation of the carcass in the scanner, there can for some of the loins be divergence between the sides measured with ultrasound and with the manual inspection. Due to the symmetry of the carcass, however, this is not a critical issue. No attempt of marking the longitudinal position of the manual inspection on the carcasses for the ultrasound data acquisition has been made. This introduces a consequential limit to the segmentation success.

Figure 1 shows a longitudinal Autofom image, which has been resized from the original size of 200×635 to 600×318 to improve the interpretation. The vertical lines in the image denote the region of 5 pixel columns where the MSD is found. The pixel rows in this region are averaged for all 16 longitudinal images, and the 3D data sequence is thereby reduced to a 16×635 transverse image. Figure 2a shows this image after a pixel replication to obtain an image of size 318×318, and the problem with the low resolution in the vertical direction is clearly visible. To meet the problems of the low vertical resolution, the images are instead resized to 318×318 using bipolar interpolation as showed in Figure 2b. This is an approach to obtain subpixel accuracy, although no new information is obtained. The images display the mid-line of the carcass at approximately 2/3rd to the right of the image. Around the mid-line, two round black structures are slightly apparent. These are the structures of the loin, and the dark region area of the left of the mid-line is (in this example) the aim of the segmentation.

Figure 3 shows the two examples of the transverse images. The top image is with a LMA of 5.75 inch^2 and the bottom image is with a LMA of 9.80 inch^2 measured with the manual method. The round dots denote the initial points found with the morphological detection. The detection of the initial points is generally reasonably accurate, but problems do occur at the weak intersection between the loin and the mid-line of the carcass. This is especially observed for the points to the right of the top image of Figure 3. In two occasions the detection of the initial points fail totally due to the morphology, and these images are removed from the succeeding segmentation trials.

The results of the elliptic fitting to the initial 16 points are seen in Figure 3. As expected from the initial points estimation, the two images are easily separated by the area of the ellipse. The segmentation is performed on three neighbouring transverse images, and the ellipse area is averaged over the three results. Table 1 presents the correlation values between the manually measured LMA and the ellipse areas for both the averaged estimates and the single estimation. A correlation of 0.68 is obtained for one transverse image only. Averaging the areas calculated on three transverse images, the correlation with LMA seems to improve slightly to r=0.70.

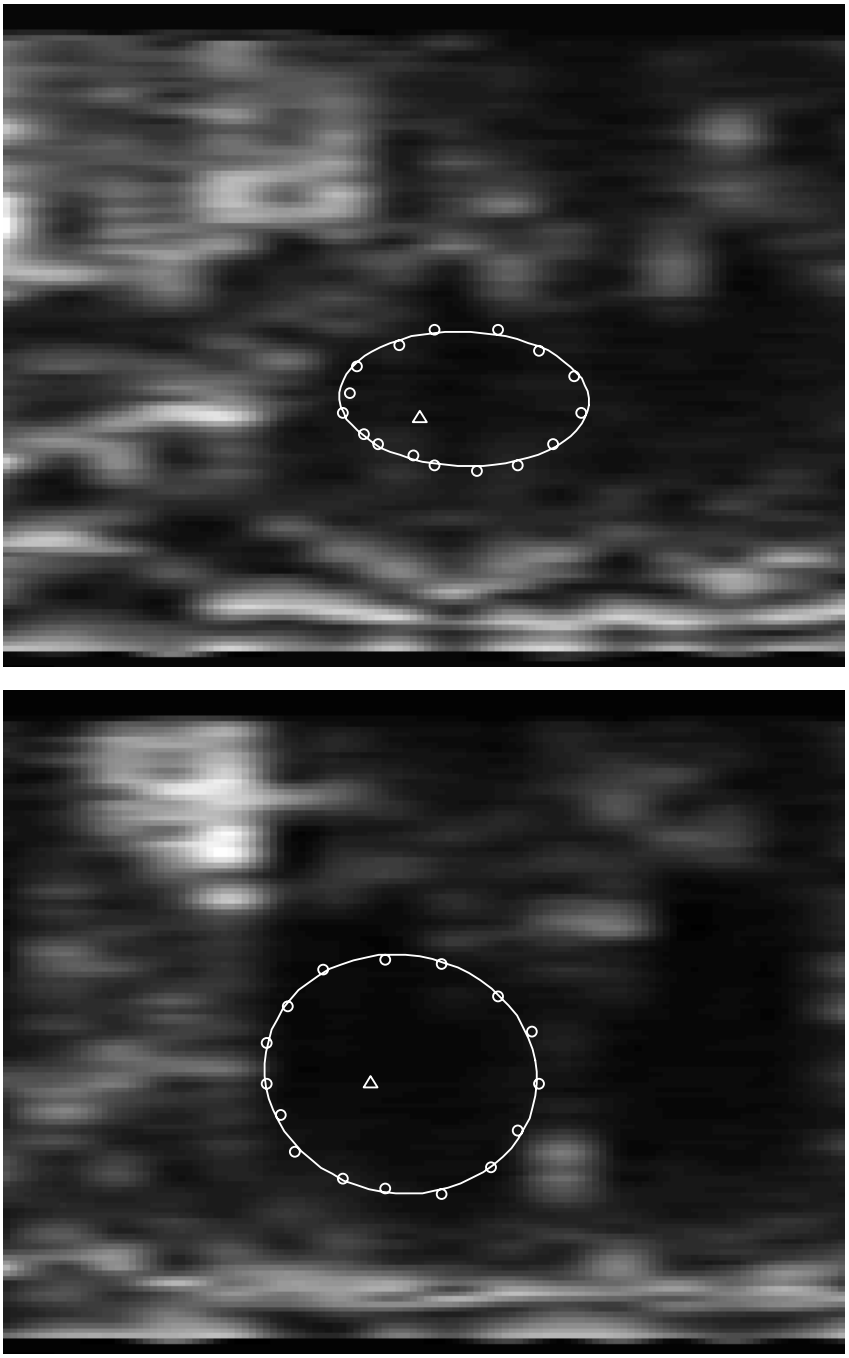

Figure 3. The ellipse fit segmentation of two images. The top image is from a carcass with LMA=5.90 inch^2, and the bottom image is with a reference LMA=9.80 inch.^{2}. The dots denote the positions of the initial points found by the morphological approach. The triangle marks CLM.

Table 1. Correlation coefficients (r) between visually measured LMA and the segmentation features (N=100).

	Ellipse (16 points)	Active contour (16 points)	Active contour (24 points)
Using CLM	0.68	0.71	0.72
Averaging 3 around CLM	0.70	0.74	0.75

The images are aligned based on the CLM point and the score image shown in Figure 4 is calculated with a PCA based 50 of the transverse images. The score image clearly shows the common muscle structure as the dark region in the centre of the image, and the increasing variation towards the outer edges of the muscle.

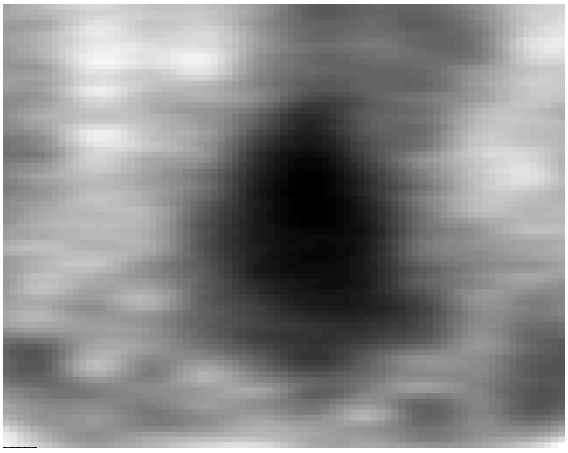

Figure 4. A score image obtained with a PCA of 50 transverse images aligned by CLM.

The results of the active contour segmentation of the two example images are shown in Figure 5a and 5b. The results have been obtained with α, λ, and ε each set to 1/3 in order to weight the three factors in equation 9 equally. The curve has been estimated from 16 vertices and 10 iterations have been used. It is observed from especially Figure 5a that the active contour tends to overfit to the edges in the image. Therefore the curvature of the contour is prioritised higher in the energy minimisation, and α is set to 0.50, and λ and ε are set to 0.25. The results of the new segmentation for the same two images are shown in Figure 6, and a more realistic loin shape is characterised by the contours.

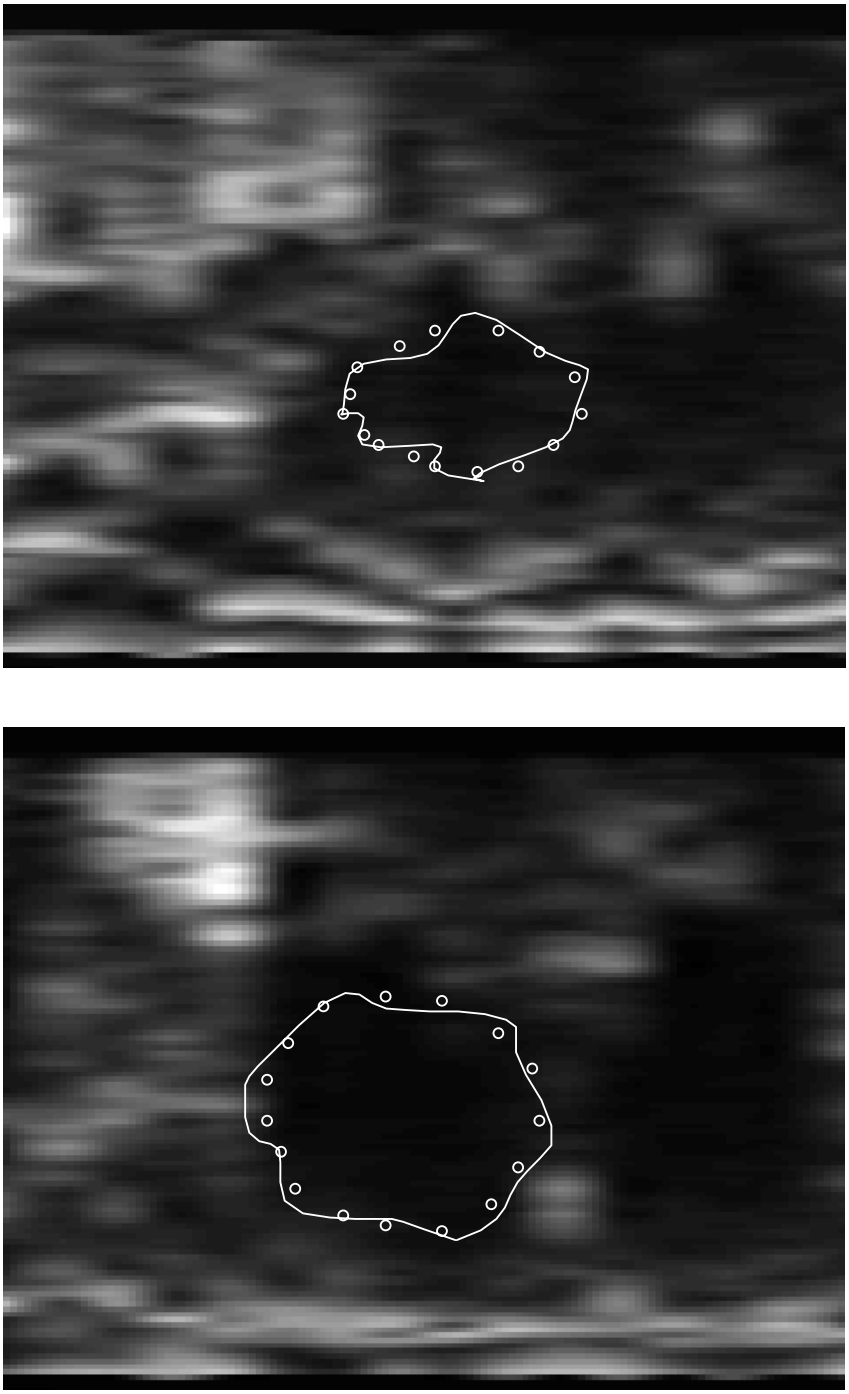

Figure 5. The active contour segmentation of two images with α=0.67, β=0.33, and γ=0.33. The top image is from a carcass with LMA=6, and the bottom image is with a reference LMA=9. The dots denote the positions of the initial points found by the morphological approach.

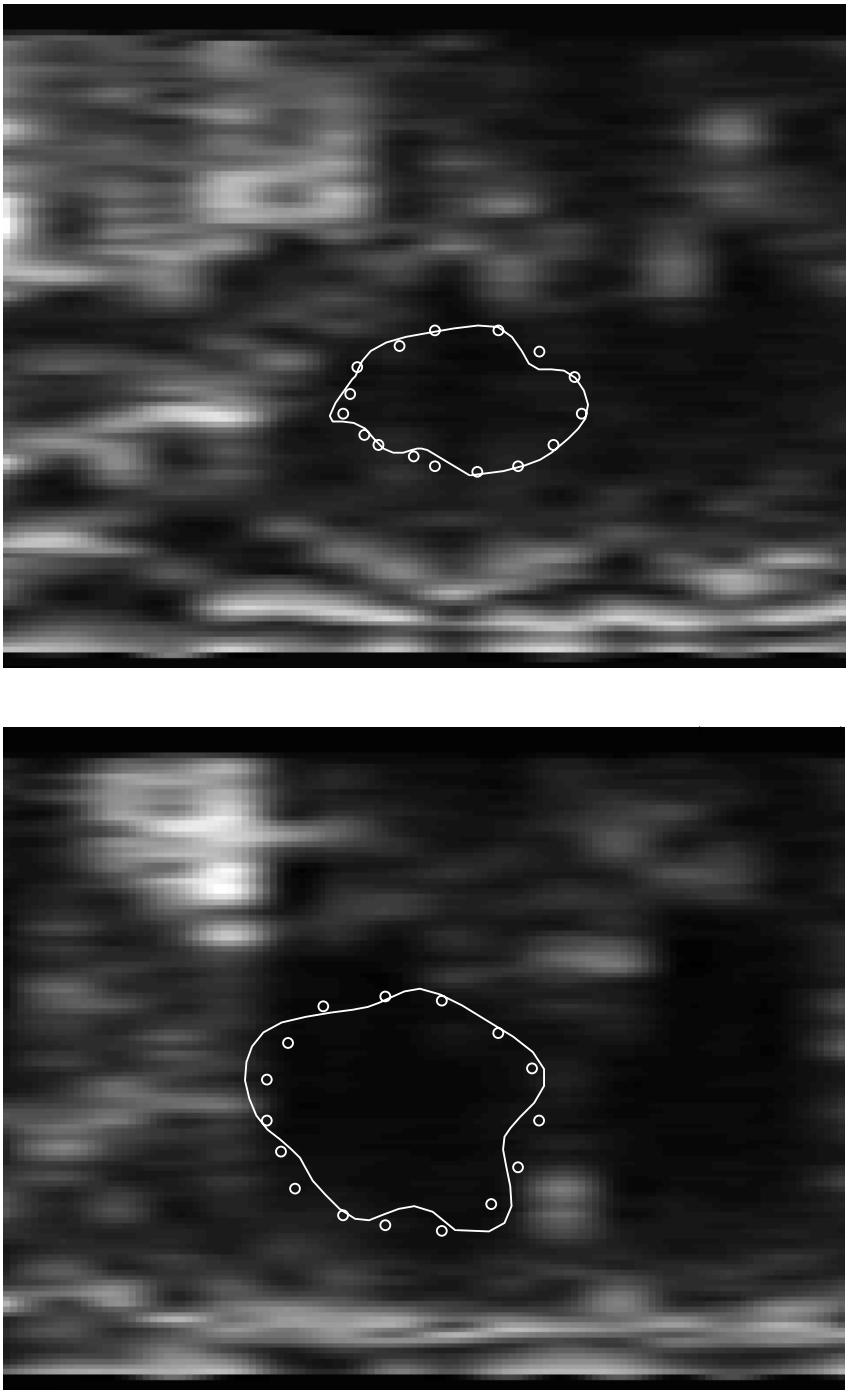

Figure 6. The active contour segmentation of two images with α=0.33, β=0.33, and γ=0.33. The top image is from a carcass with LMA=6, and the bottom image is with a reference LMA=9. The dots denote the positions of the initial points found by the morphological approach

Similar to the elliptic fit, the active contour segmentation has been performed on three neighbouring transverse images and the estimated LMA are averaged over the three results. The correlation between the area of the contour and the manually measured LMA is shown in Table 1 for both the middle contour and for the average of the neighbouring images. The correlation is seen to increase from r=0.71 to 0.74 by averaging three segmentation results. The same observation was made for the elliptic fit, and this indicates a potential improvement by measuring more locations although the improvement tends to be minimal.

Using 24 vertices instead of 16 improves the results slightly from r=0.74 to 0.75 for the average of three transverse images (Table 1). The correlation plot of the manual LMA and the averaged contour area is shown in Figure 7.

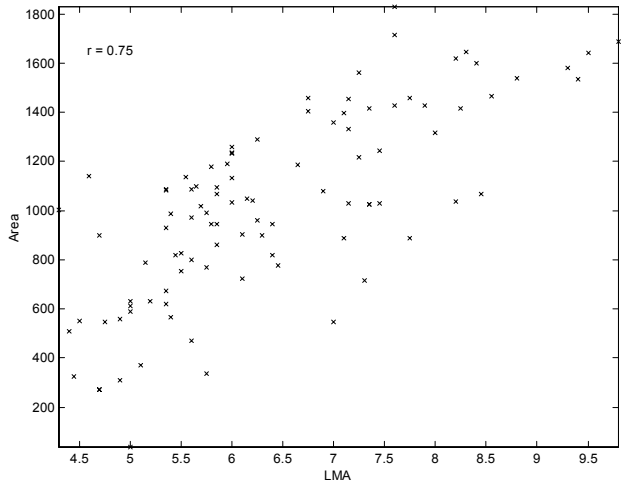

Figure 7. Scatterplot of the measured LMA versus the area of the active contour based on 24 points.

The Autofom outputs 127 features mostly focused on the skin, fat and muscle depths of the longitudinal images (Brøndum *et al.* 1998). These features and the carcass weight are included along with the segmentation parameters in a multivariate Partial Least Squares Regression (PLSR; Martens an Næs 1992) on the manual LMA measures. The PLSR is validated with two approaches. Firstly, full cross (leave one out) validation is performed, and secondly, a separation between a training set and a test set each consisting of 49 samples are formed. Table 2 present the correlation coefficient (r), standard error of prediction (SEP), and number of principal components (PC) of the PLSR results for both validation methods.

Table 2. Correlation coefficients (r), standard error of prediction (SEP) and number principal components (PC) for PLS predictions of LMA validated with cross validation ("leave one out") and test set.

	Cross validation (N=98)			Test set validation (N_{train}=49, N_{test}=49)		
	r	SEP	PC	r	SEP	PC
Autofom	0.71	0.92	2	0.61	0.88	1
Autofom + carcass weight	0.75	0.85	2	0.67	0.81	1
Autofom + active contour	0.75	0.86	1	0.75	0.74	1

As observed from Table 2, the combination of the Autofom with the carcass weight or the active contour information improves the cross validated predictions slightly. The effect from the segmentation and the weight tends to be similar. Observing the test set validation, the picture changes slightly, though. The prediction performance of the Autofom and the active contour segmentation combined, are at the same level as for the cross validation. However, the Autofom alone and also combined with the weight information is less accurate than the active contour segmentation. This indicates, that the active contour segmentation is more stable and optimised with respect to the LMA than the longitudinal Autofom parameters.

The automatic segmentation matches manual inspection of the images quite well as indicated by Figure 7. The current accuracy is limited by three factors: the resolution in the transverse ultrasound images, the correspondence between the location of the manual measurement and the Autofom measurement, and the accuracy of the manual grid measurement. Therefore, no more improvements can be expected with the current test set up. Further improvements are more likely to be expected by reducing these error sources.

Regarding the future perspectives of the segmentation method, then the on-line implementation is realistic. The algorithm is currently executed in few seconds on a standard PC, but implementation on the workstation included in the Autofom system will expectedly execute the algorithm in considerably less than one second. Another potential use of the ideas is to use the active contour principle to segment the muscle structure in succeeding image slices of the Autofom image sequence. The muscle contour detected in one image is used as the initial curve in the following image, and the active contour principle is used to update the segmentation. The focal point of this paper has the two-dimensional segmentation , but the implementation of the approach in 3D is possible using e.g. Parafac/Tucker3 (Henrion 1994).

REFERENCES

Blake, A., Curwen, R., and Zisserman, A. (1993). Affine-Invariant Contour Tracking with Automatic Control of Spatiotemporal Scale. *Proc.Int.Conf.Comp.Vision* , 66-75.

Brøndum, J., Egebo, M., Agerskov, C., and Busk, H. (1998). Carcass Grading with the Autofom Ultrasound System. *J.Anim.Sci.* **76**, 1859:1868.

Caselles, V., Kimmel, R., and Guillermo, S. (1997). Geodesic Active Contours. *Int.J.of Computer Vision* **22**(1), 61-79.

Cohen, L. D. (1991). Note: On active contour models and balloons. *CVGIP: Image Understanding* **53**(2), 211-218.

Cohen, L. D. and Cohen, I. (1993). Finite-element methods for active contour models and ballons for 2-D and 3-D images. *IEEE Transactions on Pattern Analysis and Machine Intelligence* **15**(11), 1131-1147.

Esbensen, K. H. and Geladi, P. (1989). Strategy of multivariate image analysis (MIA). *Chemometrics and Intelligent Laboratory Systems* , 67-86.

Geiger, D., Gupta, A., Costa, L. A., and Vlontzos, J. (1995). Dynamic programming for detecting and matching deformable contours. *IEEE Transactions on Pattern Analysis and Machine Intelligence* **17**(3), 294-302.

Geladi, P., Isaksson, H., Lindqvist, L., Wold, S., and Esbensen, K. H. (1989). Principal component analysis of multivariate images. *Chemometrics and Intelligent Laboratory Systems* **5**, 209-220.

Gonzalez, R.C. and Woods, R.E. (1992). *Digital image processing*, Addison-Wesley, US.

Gunn, S. R. and Nixon, M. S. (1997). A robust snake implementation; A dual active contour. *IEEE Transactions on Pattern Analysis and Machine Intelligence* **19**(1), 63-68.

Henrion, R. (1994). N-way principal component analysis. Theory, algorithms and applications, *Chemometrics and Intelligent Laboratory Systems* **25,** 1-23.

Hotelling, H. (1933). Analysis of complex statistical variables into principal components. *J.Educ.Psychol.* **24**, 417,498-441,520.

Kass, M., Witkin, A., and Terzopoulos, D. (1988). Snakes: Active Contour Models. *Int.J.of Computer Vision* **1**, 321-331.

Lai, K. L. and Chin, R. T. (1995). Deformable Contours: Modeling and Extraction. *IEEE Transactions on Pattern Analysis and Machine Intelligence* **17**(11), 1084-1090.

Martens, H. and Naes, T. (1993). Multivariate Calibration. 2ed. Wiley, New York

Mouroutis, T., Roberts, S. J., and Bharath, A. A. (1998). Robust cell nuclei segmentation using statistical modelling. *Bioimaging* **6**, 79-91.

Pearson, K. (1901). On lines and planes of closest fit to systems of points in space. *Phil.Mag.* **2**, 559-572.

Russ, J. C. (1994). The Image Processing Handbook. CRC Press.

Sapiro, G. and Tannenbaum, A. (1993). Affine Invariant Scale-Space. *Int.J.of Computer Vision* **11**(1), 25-44.